Journal of Wind Engineering & Industrial Aerodynamics 211 (2021) 104566

Contents lists available at ScienceDirect

Journal of Wind Engineering & Industrial Aerodynamics

journal homepage: www.elsevier.com/locate/jweia

Parametric flutter analysis of bridges stabilized with eccentric wings

Uwe Starossek [a,*], Rudolf T. Starossek [b]

[a] Hamburg University of Technology, Denickestr. 17, 21073 Hamburg, Germany
[b] Werner Sobek New York Corp., 180 Varick Street, New York, NY 10014, USA

ARTICLE INFO

Keywords:
Aeroelastic instability
Passive vibration control
Aerodynamic damping device
Fixed wing
Finite element flutter analysis
Parameter study
Design strategy

ABSTRACT

The eccentric-wing flutter stabilizer is a passive aerodynamic device for raising the flutter speed of a bridge. It consists of wings running parallel to the bridge deck. In contrast to similar devices proposed in the past, the wings do not move relative to the bridge deck and they are positioned outboard the bridge deck to achieve a greater lateral eccentricity. This enables the wings to produce enough aerodynamic damping to effectively raise the flutter speed. A comprehensive parametric flutter analysis study is presented in which both the properties of the bridge and the configuration of the wings are varied. The bridge properties and the wing configuration are each summarized in four non-dimensional quantities. The parameter space within which these numbers are varied are determined on the basis of previous work and the structural properties of actual long-span bridges. As for the wind forces, a streamlined bridge deck contour is assumed. The main interest of this study is the relative flutter speed increase due to the wings. This and other non-dimensional results are presented in diagrams and discussed. Both multi-degree-of-freedom and generalized two-degree-of-freedom flutter analyses are performed. Torsional divergence is addressed. A strategy for choosing a cost-efficient wing configuration is suggested.

1. Introduction

Flutter is a criterion governing the design of long-span bridges. Various measures have been proposed to raise the flutter resistance of bridges, that is, their critical wind speed for flutter onset (flutter speed). The twin deck concept was described by Richardson (1981) and has been implemented in a few bridges. It is a passive aerodynamic measure that takes advantage of the gap between the two or more bridge decks. It means additional cost due to the cross beams required to connect the individual decks. Diana et al. (2007) examined the effect of winglets positioned above the bridge deck edges without a distinct vertical or horizontal offset. Only qualitative indications were given concerning the impact of such devices on the flutter speed. Raggett (1987) and Liu et al. (2006) suggested wings that are rigidly mounted at a certain vertical distance above the bridge deck edges. The present study shows that the impact of such a configuration on flutter is small.

An active aerodynamic device for raising the flutter speed was proposed by Ostenfeld and Larsen (1992). It consists of wings, installed along the sides of the bridge deck, the pitch of which is controlled by actuators. Hence the safety of the bridge would depend on energy supply and the proper functioning of control software and hardware – a condition that meets resistance due to reliability and durability concerns. A passive aerodynamic-mechanical device described by Starossek and Aslan (2008) likewise includes variable-pitch wings along the sides of the bridge deck. Instead of being controlled by actuators, the pitch of the wings follows the movements of tuned mass dampers inside the bridge deck to which the wings are coupled. Although the safety of the bridge would not depend on energy supply and a control system, the device still includes moving parts, which raises the threshold of acceptance.

In view of these developments, it seems promising, for raising the flutter speed of a bridge, to develop immovable passive aerodynamic devices, which nevertheless are sufficiently effective without implying substantial additional cost such as the cross beams in the twin deck concept. The eccentric-wing flutter stabilizer possibly meets these requirements. It consists of wings running parallel to the bridge deck (Fig. 1). In contrast to similar devices proposed in the past and described abobe, the wings do not move relative to the bridge deck and they are positioned outboard the bridge deck to achieve a greater lateral eccentricity with regard to the bridge axis. This is accomplished by connecting the wings to the bridge deck by means of lateral cantilever support structures.

The wings produce aerodynamic damping of the bridge deck motion, particularly of the rotational motion component. This can easily be comprehended under the assumption of quasi-stationary flow. When the

* Corresponding author.
E-mail addresses: starossek@tuhh.de (U. Starossek), rudolf.starossek@wernersobek.com (R.T. Starossek).

https://doi.org/10.1016/j.jweia.2021.104566
Received 9 October 2020; Received in revised form 12 February 2021; Accepted 13 February 2021
Available online xxxx

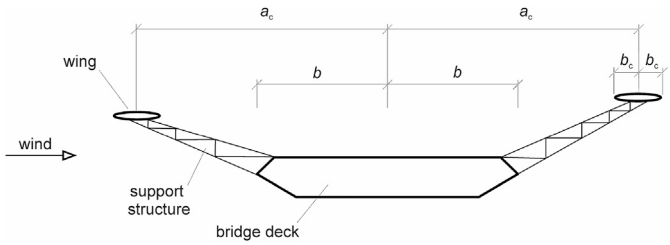

Fig. 1. Bridge deck with eccentric-wing flutter stabilizer – cross section.

vertical velocity of a wing resulting from the rotational velocity of the bridge deck is superimposed on the horizontal wind velocity, an apparent angle of attack is formed, which results in a lift force on the wing, which produces a moment on the bridge deck. This moment is in counter-phase to the rotational velocity of the bridge deck and hence corresponds to damping. This holds equally for a windward wing and a leeward wing. The additional aerodynamic damping produced by the wings raises the flutter speed. Because both the vertical velocity of a wing and the moment produced by a given lift force increase linearly with the wing's eccentricity, a_c, the wing-produced aerodynamic damping of the rotational motion of the bridge deck increases quadratically with the eccentricity of the wings. Consequently, the wings are the more effective the larger their eccentricity.

The flutter suppression effectiveness of eccentric wings was confirmed by wind tunnel tests and flutter analyses (Starossek et al., 2018), (Meyer, 2019). Its cost was investigated on the basis of design studies for the wings and their support structures and was found to be competitive (Starossek et al., 2018).

The study of flutter suppression effectiveness in (Starossek et al., 2018), (Meyer, 2019) was done for a variety of wing configurations, including configurations with different windward and leeward wings, but only for a few different bridges. Further studies have shown that the increase in flutter speed achieved by the wings is particularly sensitive to the properties of the bridge. Therefore, comprehensive parametric flutter analyses have been performed in which both the properties of the bridge and the configuration of the wings are varied. The results, limited to configurations with identical wings on both sides of the bridge deck, are presented here.

The study is based on classical bridge flutter theory. Steady-state harmonic vibration is assumed and studied in the frequency domain. The oncoming wind is assumed to be non-turbulent. The motion-induced lift forces and aerodynamic moments are linearly related to vertical displacements and rotations, and the respective velocities and accelerations, by non-stationary aerodynamic coefficients (Theodorsen, 1934). Aerodynamic interference between the windward and leeward wings and the bridge deck is neglected so that the theory can be applied separately to each of these three elements. In practice, interference can be prevented by positioning the wings above or below the bridge deck with sufficient vertical offset to the bridge deck and between them. When the oncoming wind is turbulent, its action on the wings may affect the buffeting response of the bridge. However, it has been found that the response of the bridge to buffeting, and also to vortex shedding, is mostly reduced when wings are added (Meyer, 2019). This can be ascribed to the aerodynamic damping produced by the wings, which not only is the main source of their flutter suppression effectiveness but reduces vibrations due to any kind of excitation. Given the strong flutter speed increase provided by the wings, torsional divergence can become governing over flutter. This is addressed to some extent.

For greater generality, the input data and results are presented as non-dimensional quantities. With respect to the non-dimensional flutter speed, the relevant structural properties of the bridge can be summarized in four key parameters: frequency ratio, structure-to-air mass ratio, reduced mass radius of gyration, and damping parameter. The parameter space within which these numbers are varied is determined by considering actual or planned long-span bridges. The configuration of the wings can likewise be summarized in four numbers: relative wing eccentricity, relative wing width, relative wing length, and relative wing mass. These parameters are varied on the basis of the previous studies documented in (Starossek et al., 2018). Further key parameters are the aerodynamic contours of bridge deck and wings. The results presented here are obtained on the assumption of streamlined contours using the non-stationary aerodynamic coefficient functions derived by Theodorsen (1934) and compiled by Starossek (1992). In addition to the non-dimensional flutter speed, the results are presented as the relative flutter speed increase due to the wings.

Multi-degree-of-freedom (MDOF) flutter analyses are performed. The various systems are modelled with a specially developed finite aeroelastic beam element capable of simultaneously modelling the bridge deck and the wings. Thus, the variability of the wing length can accurately be taken into account (Starossek and Starossek, 2021). The procedure is implemented in a FORTRAN program. Given the abundance of program runs to be performed, the inputs for the FORTRAN program are automatically generated by MATLAB code, which also performs the sequence control and evaluates and compiles the outputs. Additionally, generalized two-degree-of-freedom (2-DOF) flutter analyses are performed for a few selected cases using a quasi-stationary approach for taking into account the wind forces on the wings. The validity of the analytical approaches for determining the flutter speed has been confirmed by wind tunnel tests (Starossek et al., 2018).

The results are presented in diagrams and discussed extensively. The influence of the various parameters on the flutter speed increase due to the wings is emphasized. On this basis, a strategy for choosing a cost-efficient wing configuration for achieving a required flutter speed is suggested.

2. Input data

2.1. Bridge properties

2.1.1. Key parameters

Flutter theory was originally based on a generalization of the actual structural system to a system with two degrees of freedom: heave and rotation. In such a 2-DOF flutter analysis, the *structural* properties of a bridge can be summarized in four non-dimensional and two dimensional quantities (Starossek, 1992). The non-dimensional quantities are 1) the *frequency ratio*, ε, defined as

$$\varepsilon = \frac{\omega_\alpha}{\omega_h} \tag{1}$$

where ω_α = natural circular frequency of torsional vibration, and ω_h = natural circular frequency of vertical bending vibration, of an undamped bridge system without wings in a vacuum (without aerodynamic forces), both mostly associated with the lowest symmetric or lowest antisymmetric modes of vibration, whichever governs flutter, 2) the (structure-to-air) *mass ratio*, μ, defined as

$$\mu = \frac{m}{\pi\rho b^2} \tag{2}$$

where m = mass per unit length, ρ = air density, b = half chord of aerodynamic contour of bridge deck, 3) the *reduced mass radius of gyration*, r, defined as

$$r = \frac{1}{b}\sqrt{\frac{I}{m}} \tag{3}$$

where I = mass moment of inertia per unit length, and 4) a parameter that quantifies the inherent structural damping. For the latter, the *damping parameter* g is chosen: the damping forces are assumed to be g times the elastic restoring forces acting with a phase shift of 90° so that

they are in counter-phase to velocity (Försching, 1974).

Properties m and I refer to the bridge deck plus, if present, the suspension cables. (More generally, they are generalized properties related to the distributed mass of the system by the respective mode of vibration). They do not include the mass of the wings, which is part of the wing parameters and specified separately.

The dimensional structural quantities used to compute the flutter speed are b and ω_h. These quantities are not varied in this study given that the non-dimensional flutter speed, which is of interest here, is independent of them.

The above choice of flutter-relevant input parameters is not the only possible one. Other four non-dimensional and two dimensional quantities could be chosen as long as they are independent of each other and capture the relevant structural properties of the bridge. For instance, the reduced mass radius of gyration, r, could be replaced, as an independent parameter, by the mass moment of inertia ratio, μr^2.

The flutter speed also depends on the *aerodynamic contour* of the bridge deck, which is another key parameter in addition to the structural properties.

2.1.2. Choice of parameter values

Key parameters of actual or planned long-span bridges are compiled as a basis for making a meaningful choice of the values to assign to these parameters in the analysis. Table 1 gives an overview of this empirical data.

The table shows the natural cyclic frequencies of vertical and torsional vibration, f_h and f_α, that are associated with the lowest symmetric or lowest antisymmetric modes of vibration. The combination of modes listed here are those that govern flutter according to a 2-DOF analysis using Theodorsen's non-stationary aerodynamic coefficients. The respective kind of modes is indicated by "sym" or "anti." The references indicate the sources. With respect to the first Tacoma Narrows Bridge, the mass and the mass moment of inertia given in the literature differ from one another and are inconclusive. Therefore, these properties have been determined by the authors based on the design drawings reproduced in (Farquharson et al., 1949). They include the mass contribution of the suspension cables (as for all suspension bridges listed here). The torsional frequency $f_\alpha = 0.233$ Hz was observed on the morning of the collapse. Immediately before collapse, this frequency changed to $f_\alpha = 0.200$ Hz. The mass moment of inertia of the Great Belt Bridge was estimated based on (Larsen and Jacobsen 1992), (Larsen, 1993) and (Ewert, 2003), the one of Xihoumen Bridge based on (Yang et al., 2018), and the one of Ponte di Messina based on (Brancaleoni et al., 2010). The mass and the mass moment of inertia of Akashi Kaikyo Bridge were estimated based on (Brancaleoni et al., 2010), (Ewert, 2003) and (Fuchida et al., 1998). The mass and the mass moment of inertia of Tatara Bridge were estimated based on (Yanaka et al., 1998); they do not include the stay cables.

Based on this data, the main values assigned to parameters ε, μ, and r are chosen as follows.

$$\varepsilon = 1.3;\ 1.7;\ 2.3;\ 3.0 \tag{4}$$

$$\mu = 15;\ 25;\ 40;\ 60 \tag{5}$$

$$r = 0.7;\ 0.8;\ 0.9 \tag{6}$$

Furthermore, ε is varied from 1.00 to 3.00 in 0.01-increments for selected combinations of values of the other parameters.

Structural damping consists of different energy dissipation mechanisms which are mostly all modelled as viscous damping and quantified as damping ratio-to-critical, ξ. There is a great variability of published values of ξ for bridges. A mean value of 1.25% and a lower bound value of 0.5% is reported in (Salcher et al., 2014) for long-span steel bridges. In view of the uncertainty regarding damping, only one value is considered here in addition to the no-damping condition. The analyses performed for this study show that structural damping reduces the relative flutter speed increase slightly in some cases, but raises it strongly in other cases (see Section 4.3 and Fig. 8). Therefore, the value of the damping parameter of the damped system is chosen as $g = 0.01$, which corresponds to the lower-bound value $\xi = 0.5\%$ (see Eq. (20)). The values considered are thus

$$g = 0;\ 0.01 \tag{7}$$

As for the aerodynamic contour, this study focuses on bridges with streamlined decks.

2.2. Wing configurations

2.2.1. Key parameters

When identical wing configurations are chosen on both sides of the bridge deck, which is always the case in this study, the properties of the wings can likewise be summarized in four non-dimensional quantities, that is, 1) the *relative wing eccentricity*, $\tilde{a}_c$, defined as

$$\tilde{a}_c = \frac{a_c}{b} \tag{8}$$

where a_c = eccentricity of a wing relative to bridge deck axis (centre-to-centre distance), 2) the *relative wing width*, $\tilde{b}_c$, defined as

Table 1
Key parameters of long-span bridges.

	1st Tacoma Narrows Bridge		Great Belt Bridge		Xihoumen Bridge		Ponte di Messina		Akashi Kaikyo Bridge		Tatara Bridge	
		note		note		note		note		note		note
f_h [Hz]	0.145	Farquharson et al. (1949)	0.0999	Larsen and Jacobsen (1992)	0.1005	Yang et al. (2018)	0.06031	Brancaleoni et al. (2010)	0.1015	Miyata et al. (1992)	0.223	Yamaguchi et al. (2004)
f_α [Hz]	0.233	Farquharson et al. (1949)	0.278	Larsen and Jacobsen (1992)	0.2321	Yang et al. (2018)	0.07994	Brancaleoni et al. (2010)	0.2383	Miyata et al. (1992)	0.497	Yamaguchi et al. (2004)
ε	1.61	anti	2.78	sym	2.31	sym	1.33	anti	2.35	sym	2.23	sym
b [m]	5.94	Farquharson et al. (1949)	15.5	Larsen and Jacobsen (1992)	18.0	Yang et al. (2018)	30.575	Brancaleoni et al. (2010)	17.75	Miyata et al. (1992)	15.3	Yanaka et al. (1998)
m [t/m]	8.19		22.7	(Larsen, 1993)	25.0	Yang et al. (2018)	49.7	Brancaleoni et al. (2010)	36.2		15.1	
I [tm^2/m]	202.4		3537		3932		31,520		8507		2096	
μ	60.3		24.6		20.1		13.8		29.9		16.8	
r	0.837		0.805		0.697		0.824		0.864		0.770	

$$\tilde{b}_c = \frac{b_c}{b} \tag{9}$$

where b_c = half chord of a wing, 3) the *relative wing length*, $\tilde{L}_c$, defined as

$$\tilde{L}_c = \frac{L_c}{L} \tag{10}$$

where L_c = total length of wings on one side of bridge deck, L = total length of bridge, and 4) the *relative wing mass*, $\tilde{m}_c$, defined as

$$\tilde{m}_c = \frac{m_c}{m} \tag{11}$$

where m_c = mass per unit length of wings on one side of bridge deck (possibly including a contribution of the support structures). The quantities a_c, b_c, m_c and their non-dimensional equivalents are assumed to be constant along the length of the wings.

When $\tilde{L}_c < 1$, it is assumed that the wings are centred in relation to the peak positions of the governing mode shapes. Such a positioning leads to maximum effectiveness. In a symmetric three-span suspension bridge with flutter being governed by the lowest symmetric modes of vibration, the wings would be placed contiguously and centred in relation to the main span centre.

Another freedom of design would be to choose different wing configurations on either side of the bridge deck. This could be beneficial if the expected maximum wind speeds from either transverse direction differ strongly. The flutter suppression effectiveness of the wings also depends on their *aerodynamic contour*, which is hence another key parameter in addition to the structural properties.

2.2.2. Choice of parameter values

Based on previous studies of the flutter suppression effectiveness of the wings and of the design and cost of wings and support structures (Starossek et al., 2018), the main values assigned to parameters $\tilde{a}_c$, $\tilde{b}_c$, $\tilde{L}_c$, and $\tilde{m}_c$ are chosen as follows.

$$\tilde{a}_c = 2.0 \tag{12}$$

$$\tilde{b}_c = 0.1 \tag{13}$$

$$\tilde{L}_c = 0;\ 1 \tag{14}$$

$$\tilde{m}_c = 0;\ \left(0.015 \cdot \tilde{b}_c \Big/ 0.1\right) \tag{15}$$

Furthermore, $\tilde{a}_c$ is varied from 1 to 2.5 in 0.01-increments, $\tilde{b}_c$ from 0 to 0.15 in 0.001-increments, and $\tilde{L}_c$ from 0 to 1 in 0.04-increments, for selected combinations of values of the other parameters.

The effects of choosing different wing configurations for each side of the bridge deck is left for future studies and it is assumed here that the wing configuration is symmetric with respect to the bridge deck centre line (except for the vertical offset between the windward and leeward wings). The wings are aerodynamically shaped so that they generate large lift forces and drag and wake are small. Their flutter suppression effectiveness is thus maximized and any harmful side effects are minimized. Their contours are envisaged as streamlined elongated ellipses (Starossek et al., 2018).

3. Analysis

3.1. Assumptions

The study is based on the assumptions and uses the methods of classical bridge flutter theory. That is, steady-state harmonic vibration is assumed and studied in the frequency domain. The oncoming wind is assumed to be non-turbulent. Only motion-induced lift forces and aerodynamic moments are considered. They are linearly related to vertical displacements and rotations, and the respective velocities and accelerations, by complex aerodynamic coefficients that are functions of the degree of non-stationarity of the flow (Theodorsen, 1934). Consequently, eigenvalue problems are established and solved. Aerodynamic interference between the windward and leeward wings and the bridge deck is neglected so that non-stationary aerodynamic coefficient functions can be applied separately to each of these three elements for determining the respective motion-induced wind forces.

3.2. Model

This study aims at general applicability. Therefore, instead of focusing on a particular suspension bridge or other long-span bridge type, a simple generic system is considered that does not introduce any further variables of design: a simply supported girder with torsionally fixed ends. The definitions of key parameters in Section 2 are adopted with the following specifications. The girder forms the bridge deck. The frequencies ω_h and ω_α are associated with the lowest *symmetric* modes of vertical and torsional vibration of the generic substitute system. Properties m and I refer to the girder only and are assumed to be constant along its length. L is the span length of the girder. Identical wing configurations are present on both sides of the girder. The wings are rigidly attached to the girder and are placed contiguously and centred in relation to midspan. The aerodynamic contours of girder and wings are thin flat plates.

The latter specification allows the use of the non-stationary aerodynamic coefficient functions established by Theodorsen assuming potential flow past a thin flat plate (Theodorsen, 1934), (Starossek, 1992), independently for the girder and the wings, to take into account the respective wind forces. Theodorsen's aerodynamic coefficient functions enable a reasonable estimate of the flutter speed for airfoils and bridges with streamlined bridge deck. It is believed that accuracy is even higher for the *relative* flutter speed increase due to the wings, which is the main focus of this study. Other advantages are the benchmark character of Theodorsen's coefficients, which allow for easy comparison and verification, and greater generality by not referring to any particular bridge deck contour.

Long-span bridges are mostly not simply supported girders but are more complex in topology and articulation. Nevertheless, the results obtained for the model girder considered here are deemed representative for such bridges as long as the uncoupled (vacuum) modes of vertical and torsional vibration that govern flutter are similar to each other, as is the case for the model girder, given that generalization would then lead to the same generalized system properties. Most long-span bridges meet this condition. When applied to cable-supported bridges, the results obtained can be conservative in the case of wing configurations where wings are present but do not extend over the full length of the bridge ($0 < \tilde{L}_c < 1$). In a three-span suspension bridge, for instance, not placing wings in the side spans would not reduce the flutter suppression effectiveness of the wings by much but strongly reduce the value of $\tilde{L}_c$ used in the model analysis. In a suspension bridge, the frequencies of the lowest symmetric and lowest antisymmetric modes of vibration can be close to each other. In such a case, the results obtained here, with a simply supported girder, must be applied to both the lowest symmetric modes and the lowest antisymmetric modes of vertical and torsional vibration, and the wings, with their respective total length L_c, must be centred in relation to the peak positions of the respective mode shapes.

3.3. Method

MDOF flutter analyses are performed. The various girder-plus-wings systems are modelled with a specially developed finite aeroelastic beam element capable of simultaneously modelling the girder and the wings (Starossek and Starossek, 2021). The variability of the wing length

can thus properly be taken into account. The stiffness, mass, and aerodynamic matrices of the system, $\boldsymbol{K}$, $\boldsymbol{M}$, and $\boldsymbol{A}$ are assembled from the respective element matrices (Clough and Penzien, 1975). The system matrices are $n \times n$ matrices, where n is the number of degrees of freedom of the system. An eigenvalue problem of the form

$$\{(1+ig)\boldsymbol{K} - \omega^2[\boldsymbol{M}+\boldsymbol{A}(k)]\}\boldsymbol{\Phi} = \boldsymbol{0} \tag{16}$$

is established, where $\boldsymbol{\Phi}$ = system node displacement vector and g = structural damping parameter (Starossek, 1992), (Starossek, 1993). The structural damping represented by g is proportional to the elastic restoring forces and is in counter-phase to velocity. It is set to a value according to Eq. (7). The aerodynamic matrix, $\boldsymbol{A}$, is complex and depends on k = reduced frequency, which is a non-stationarity parameter defined as

$$k = \frac{\omega b}{u} \tag{17}$$

where ω = circular frequency of motion and u = wind speed. When $k \in \Re$ is fixed, a linear complex eigenvalue problem, with the eigenvalue ω^2, is obtained. Its solution leads to n generally complex eigenfrequencies $\omega_i = \omega_i' + i\omega_i''$, where $\omega_i' = \mathrm{Re}(\omega_i)$ and $\omega_i'' = \mathrm{Im}(\omega_i)$ are the real and imaginary parts of ω_i. The procedure is repeated for other k with the aim of identifying cases where the imaginary part ω_j'' of one eigenfrequency ω_j vanishes. The corresponding wind speed then follows as

$$u = \frac{\omega_j' b}{k} \tag{18}$$

The minimum wind speed found in this manner is the flutter speed, which in the following is likewise called u. The associated ω_j' is the circular flutter frequency, which in the following is simply called ω. To safely identify the flutter speed, the search starts with large and then decreasing values of k or small and then increasing values of $1/k$ = reduced wind speed. The governing case is usually associated with one of the lowest eigenfrequencies and hence the eigenvalue analysis can be limited to a number of lowest, say two to eight, eigenmodes.

The above approach to account for structural damping leads to the simplest form of the MDOF flutter eigenvalue problem. Equivalent viscous modal damping ratios-to-critical, ξ_i, for any eigenmode i are

$$\xi_i = \frac{g\omega_i^0}{2\omega} \tag{19}$$

where ω_i^0 = natural circular frequency of the undamped system in a vacuum associated with eigenmode i (Starossek, 1992). In the analyses performed here, ω is always found between ω_α and ω_h, that is, the natural circular frequencies associated with the vacuum eigenmodes that mainly participate in the flutter vibration. For the average equivalent viscous modal damping ratio-to-critical, ξ, thus follows

$$\xi \approx \frac{g}{2} \tag{20}$$

3.4. Details

A FORTRAN program has been developed that implements the finite aeroelastic beam element mentioned above and solves the MDOF flutter eigenvalue problem according to Eq. (16) using a vector iteration method.

The model girder is segmented into 50 identical elements leading to 199 degrees of freedom to allow variation of $\tilde{L}_c$ in 0.04-increments. Properties b and ω_h are set to $b = 1$ m and $\omega_h = 1/\mathrm{s}$, which is immaterial to the non-dimensional results presented below. The remaining input data are chosen such that the non-dimensional parameter values specified in Sections 2.1.2 and 2.2.2 are met. For the representation of ω_α and ω_h, and thus ε, the respective analytical free-vibration frequency formulae are used for determining the corresponding dimensional input quantities (leading to negligible errors due to the MDOF discretization (Starossek and Starossek, 2021)). The non-stationary aerodynamic coefficient functions given in Theodorsen (1934), Starossek (1992) are used for girder and wings. They are computed based on a rational function approximation of the Theodorsen function (Bruno et al., 1987). The number of eigenmodes to be computed was initially set to two, which proved sufficient in most cases. In a few cases, up to six eigenmodes were required to properly identify flutter.

The results presented here are based on over 30,000 FORTRAN runs, one for each combination of input parameters and resulting flutter speed. Given this abundance of runs, the input for the FORTRAN program is automatically generated by MATLAB code, which also performs the sequence control and evaluates and compiles the output. With this tool, essentially only the parameter space to be studied must be specified as user input. A spreadsheet program is used to sort and display the results.

3.5. Torsional divergence

Given that the flutter speed is increased by the wings, torsional divergence may become governing over flutter. When the same assumption of potential flow past a thin flat plate is used (as for the aerodynamic coefficient functions used for computing the flutter speed), the critical wind speed for torsional divergence (divergence speed) of the girder without wings, u_{div}, is given by (Starossek, 1992)

$$u_{\mathrm{div}} = \omega_\alpha b\sqrt{\mu r^2} \tag{21}$$

Assuming that identical wings are added on both sides of the girder along its entire length, it can be shown that the divergence speed decreases by a fraction of $\tilde{b}_c^2$, which will be neglected here.

4. Results and discussion

4.1. General

Numerical results are presented in terms of the *non-dimensional flutter speed*, ζ, and the *non-dimensional flutter frequency*, $\tilde{\omega}$, which relate the flutter speed u and the circular flutter frequency ω to system properties and are defined as

$$\zeta = \frac{u}{\omega_h b} \tag{22}$$

$$\tilde{\omega} = \frac{\omega}{\omega_h} \tag{23}$$

and in terms of the reduced frequency, k. Furthermore, the relative flutter speed increase, called the *flutter speed increase ratio*, R, is considered. It is defined as the flutter speed of the structure with wings to the flutter speed of the same structure without wings, that is,

$$R = \frac{u_{\text{with wings}}}{u_{\text{without wings}}} \tag{24}$$

and is an indicator of the flutter suppression effectiveness of the wings. The non-dimensional divergence speed, ζ_{div}, defined similarly to ζ, is

$$\zeta_{\mathrm{div}} = \frac{u_{\mathrm{div}}}{\omega_h b} = \varepsilon\sqrt{\mu r^2} \tag{25}$$

Reference is also made to the Selberg's approximation formula for the flutter speed (Selberg, 1961). Related to system properties, it reads

$$\zeta_{\mathrm{Sel}} = \frac{u_{\mathrm{Sel}}}{\omega_h b} = 0.74\sqrt{(\varepsilon^2 - 1)\mu r} \tag{26}$$

For $1.5 \leq \varepsilon \leq 3.0$, $20 \leq \mu \leq 100$, $0.75 \leq r \leq 1.00$, the formula is accurate to within 3% (Starossek, 1992).

In the following, ratios of non-dimensional speeds are also considered. These are the same as the ratios of the respective dimensional speeds as long as the non-dimensional speeds refer to the same denominator.

4.2. Girder without wings

The model girder without wings is considered first. Fig. 2 shows the non-dimensional flutter speed, ζ, of the undamped system ($g = 0$) plotted against the frequency ratio, ε, for all combinations of the chosen main values of μ and r. The flutter speed mostly increases with ε, μ, and r, a tendency reflected by Selberg's formula, Eq. (26). When ε decreases approaching the value of one, the flutter speed again increases abruptly and tends to infinity at a certain start value of ε that is always larger than one. For smaller values of ε, no flutter occurs.

Fig. 3 shows the non-dimensional flutter speed for $\mu = 15$, $r = 0.7$ and $\mu = 60$, $r = 0.9$, that is, the parameter combinations that, for most values of ε, lead to the smallest and greatest values of ζ in Fig. 2. The curves for various conditions are compiled in this diagram. The curves labelled A apply to the undamped system without wings and are the same as the respective curves in Fig. 2. The curves labelled B result when structural damping ($g = 0.01$) is added. The flutter speed increases, although the differences between curves A and B only become significant for small ε.

Another manner of presentation is chosen to better illustrate these differences. The curves in Fig. 4 represent the flutter speed of the damped system without wings divided by the flutter speed of the undamped system without wings (corresponding to "B/A," referring to the curves in Fig. 3) for the previously considered μ and r and two additional (governing) combinations. The maximum increase is found for $\mu = 15$, $r = 0.9$, the minimum increase for $\mu = 60$, $r = 0.7$. For $\varepsilon = 1.3$, the flutter speed increase due to structural damping lies between 4.4% and 8.0%; and for $\varepsilon = 3.0$, between 1.3% and 2.9%.

4.3. Girder with full-length wings – constant wing eccentricity and width

Wings are added on both sides of the girder along its entire length ($\tilde{L}_c = 1$). The relative wing eccentricity is $\tilde{a}_c = 2.0$; the relative wing width is $\tilde{b}_c = 0.1$. The curves in Fig. 3 labelled C result when neither structural damping nor the wing mass is taken into account ($g = 0, \tilde{m}_c = 0$). In comparison to curves A and B, curves C are more rounded and shifted upwards and to the right. The shift is particularly pronounced for parameter combination $\mu = 15$, $r = 0.7$. The curves in Fig. 3 labelled D result when the mass of the wings ($\tilde{m}_c = 0.015$) is taken into account, and the curves labelled E when structural damping ($g = 0.01$) is finally added. The start value of ε below which no flutter occurs increases from A to E (for all combinations of μ and r, including the ones not shown in Fig. 3).

Again, ratios are considered to better illustrate the respective differences. The curves in Fig. 5 represent the flutter speed of the undamped system with wings neglecting the wing mass divided by the flutter speed of the undamped system without wings (corresponding to "C/A," again referring to the curves in Fig. 3) now for all combinations of the chosen main values of μ and r. This ratio reflects the influence of the wings on the flutter speed and corresponds to the flutter speed increase ratio, R, for an undamped system when the wing mass is neglected. For all values of ε, R increases inversely to μ and, for values of ε smaller than a respective cross-over value, inversely to r. All curves increase with decreasing ε up to a respective start value of ε (with the chosen scaling visible only for $\mu = 15$, $r = 0.7$). For smaller ε, no flutter occurs (notwithstanding

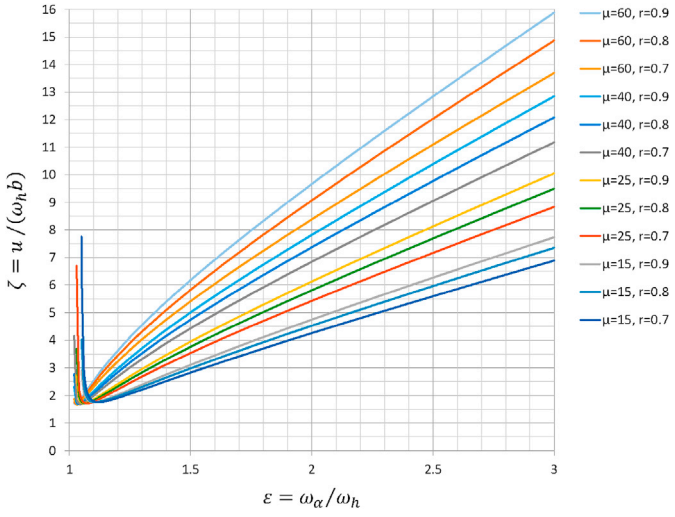

Fig. 2. Non-dimensional flutter speed, ζ, of undamped system without wings against frequency ratio, ε.

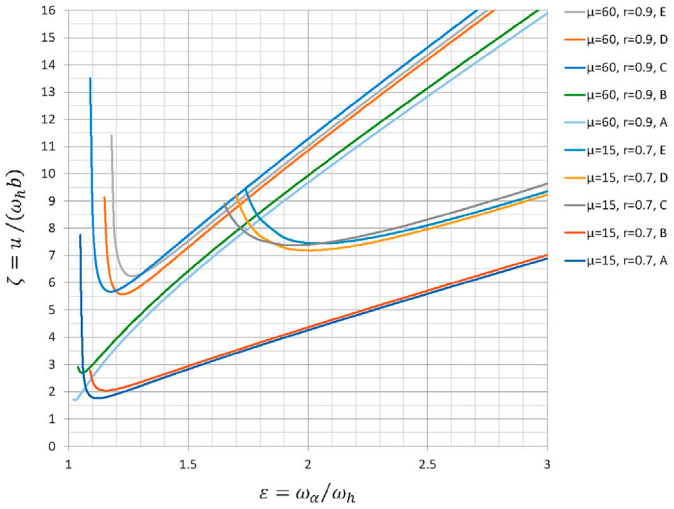

Fig. 3. Non-dimensional flutter speed, ζ, against frequency ratio, ε, for various conditions: A = no wings, undamped, B = no wings, damped, C = with wings, undamped, wing mass neglected, D = with wings, undamped, wing mass considered, and E = with wings, damped, wing mass considered.

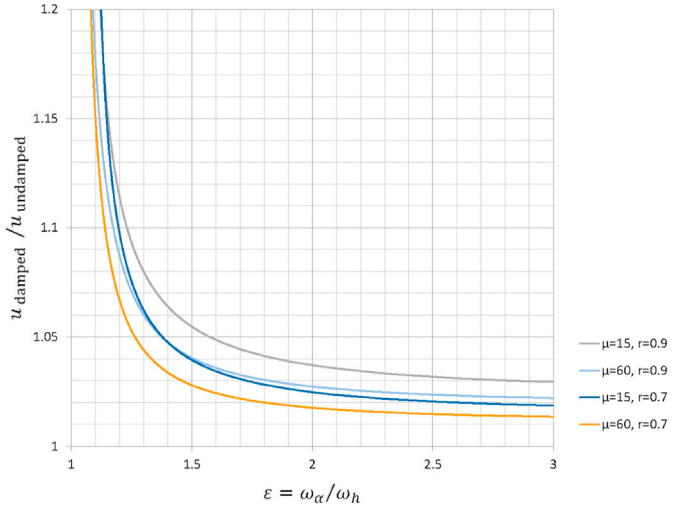

Fig. 4. Ratio of flutter speed of damped system ($g = 0.01$) to flutter speed of undamped system, both without wings, against frequency ratio, ε.

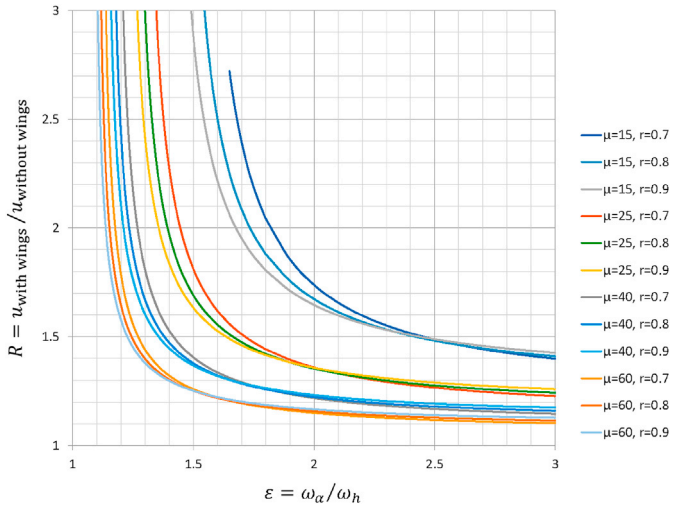

Fig. 5. Flutter speed increase ratio, R, for undamped system, wing mass neglected, against frequency ratio, ε ($\tilde{a}_c = 2.0$, $\tilde{b}_c = 0.1$, $\tilde{L}_c = 1$).

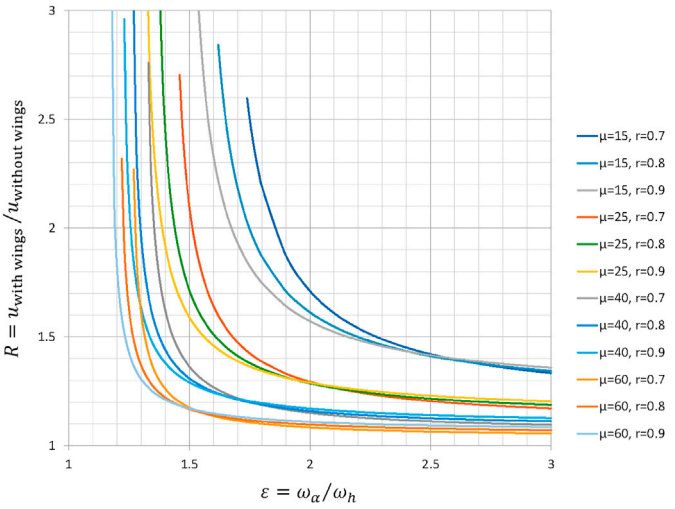

Fig. 6. Flutter speed increase ratio, R, for damped system, wing mass considered, against frequency ratio, ε ($g = 0.01$, $\tilde{a}_c = 2.0$, $\tilde{b}_c = 0.1$, $\tilde{L}_c = 1$, $\tilde{m}_c = 0.015$).

possible flutter at much higher wind speeds associated with higher modes of vibration). Significant increases of flutter speed are noted, particularly for the lower values of μ. This inverse relationship can be ascribed to the ratio of the aerodynamic damping forces, produced by the wings, to the internal system forces, due to inertia and stiffness, which becomes greater for smaller μ and thus makes the wing-produced damping more effective. The inverse relationship between R and ε seen here and also in Fig. 6 corresponds to the observation in Fig. 3 that curves A to E belonging to the same combination of μ and r are shifted not only upwards but also to the right and run essentially parallel and at the same inclination from a respective value of ε.

The curves in Fig. 6 represent the flutter speed of the damped system with wings, taking into account the wing mass, divided by the flutter speed of the damped system without wings (corresponding to "E/ B"). This ratio corresponds to the flutter speed increase ratio, R, for a damped system when the wing mass is considered. The same tendencies as in Fig. 5 are noted. Again, all curves increase with decreasing ε up to a certain start value of ε. Significant increases of flutter speed are noted. For $r = 0.8$, the flutter speed is raised by more than 50% for $\mu = 15$, $\varepsilon \leq 2.20$ / $\mu = 25$, $\varepsilon \leq 1.61/\mu = 40, \varepsilon \leq 1.38/\mu = 60, \varepsilon \leq 1.27$ and it is more than doubled for $\mu = 15$, $\varepsilon \leq 1.75$ / $\mu = 25$, $\varepsilon \leq 1.44$ /$\mu = 40, \varepsilon \leq 1.30/\mu = 60, \varepsilon \leq 1.23$. For $\mu = 15$, $r = 0.7$, the flutter speed is raised by a factor of $R = 2.60$ at $\varepsilon = 1.74$. For smaller ε, no flutter occurs. For $\varepsilon \leq 1.3$, no flutter occurs for any of the considered combinations with $\mu = 15$ and $\mu = 25$ and for the combination $\mu = 40$, $r = 0.7$, contrary to the system without wings.

The question arises to what degree the flutter speed increase ratio, R, is sensitive to the assumptions about wing mass and structural damping. Fig. 7 refers to the undamped system. The curves represent the flutter speed increase ratio when the wing mass is considered divided by the flutter speed increase ratio when the wing mass is neglected (corresponding to "(D /A)/(C /A)," again referring to the curves in Fig. 3). It is seen that the wing mass can reduce or raise the flutter speed increase ratio, and thus the flutter speed, depending on the parameter combination. For the parameter space considered here, the maximum reduction is 8.1%. It occurs for $\varepsilon = 1.45$, $\mu = 60$, $r = 0.7$. The reduction is due to the reduction of the natural frequencies due to the wing mass. On the other hand, the flutter speed is raised, partly strongly, for all values of ε below a certain root value. For $\mu = 15$, $r = 0.7$, this value is $\varepsilon = 1.85$. For $\mu = 25$, $r = 0.8$, it is $\varepsilon = 1.47$. The latter effect is related to the strong negative gradient of the $R(\varepsilon)$ curves in Fig. 5 at the beginning of these curves. When wing mass is added, the torsional natural frequency is reduced more than the vertical one (see Eqs. 28 and 29). Hence the effective frequency ratio decreases, which, for small enough ε, leads to a

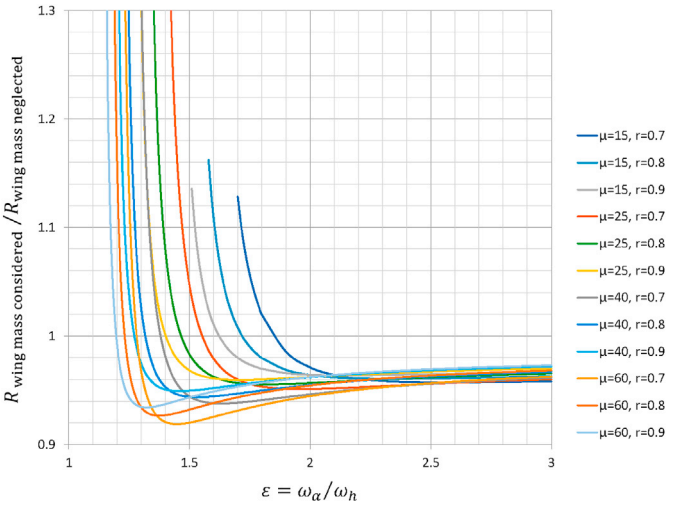

Fig. 7. Flutter speed increase ratio when wing mass considered referred to flutter speed increase ratio when wing mass neglected, for undamped system, against frequency ratio, ε ($\tilde{a}_c = 2.0$, $\tilde{b}_c = 0.1$, $\tilde{L}_c = 1$, $\tilde{m}_c = 0.015$).

higher flutter speed increase.

The curves in Fig. 8 represent the flutter speed increase ratio for the damped system divided by the flutter speed increase ratio for the undamped system when in both cases the wing mass is taken into account for the respective systems with wings (corresponding to "(E /B)/(D /A)"). It is seen that structural damping can only slightly reduce but strongly raise the flutter speed increase ratio. The maximum reduction is 1.5% reached at $\varepsilon = 3.0$, $\mu = 15$, $r = 0.9$. The flutter speed increase ratio is raised for all values of ε below a certain root value, similarly to Fig. 7. For $\mu = 15$, $r = 0.7$, this value is $\varepsilon = 2.36$. For $\mu = 25$, $r = 0.8$, it is $\varepsilon = 1.72$. The flutter speed increase ratio is raised by 15.7% at $\varepsilon = 1.3$, $\mu = 60$, $r = 0.7$. Another effect of damping is that the start value of ε below which no flutter occurs is raised, as already noted in the above discussion of Fig. 3. For $\mu = 15$, $r = 0.7$, this value increases from $\varepsilon = 1.70$ to 1.74. This effect can result in the flutter speed being raised from a finite value to infinity. The particularities observed in Fig. 8 hint at a strongly nonlinear and mostly over-proportional dependency of the flutter speed on the total damping, consisting of the structural damping plus the aerodynamic damping produced by the wings. This topic is addressed

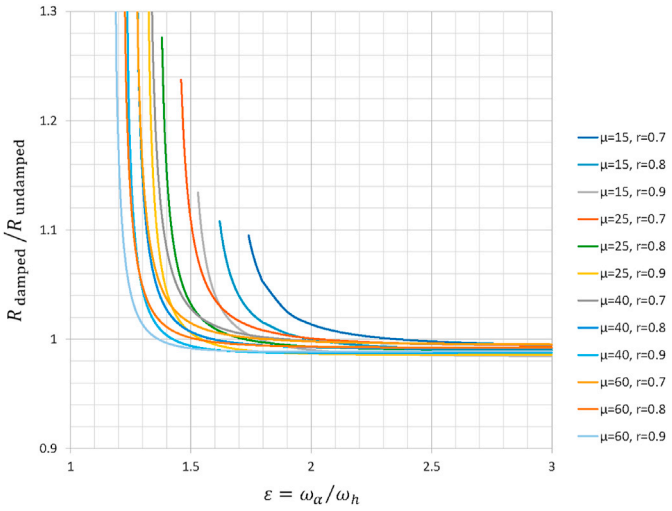

Fig. 8. Flutter speed increase ratio for damped system (g = 0.01) referred to flutter speed increase ratio for undamped system, wing mass always considered, against frequency ratio, ε ($\tilde{a}_c = 2.0$, $\tilde{b}_c = 0.1$, $\tilde{L}_c = 1$, $\tilde{m}_c = 0.015$).

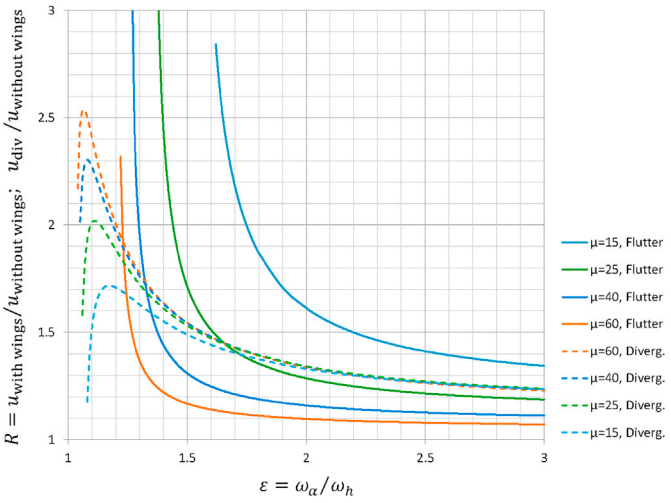

Fig. 9. Flutter speed increase ratio, R, and ratio of divergence speed to flutter speed without wings, against frequency ratio, ε ($r = 0.8$, $g = 0.01$, $\tilde{a}_c = 2.0$, $\tilde{b}_c = 0.1$, $\tilde{L}_c = 1$, $\tilde{m}_c = 0.015$).

again at the end of Section 4.6. Incidentally, a different tendency was found with uncoupled torsional flutter, in which the relative flutter speed increase due to the wings is larger the smaller the structural damping (Starossek and Starossek, 2021).

4.4. Flutter versus torsional divergence

The results so far show a strong flutter speed increase provided by the wings. Before continuing this discussion, torsional divergence shall be addressed as it may become governing over flutter. In Fig. 9, four of the curves of Fig. 6 are compared with corresponding curves that refer to the divergence speed. The comparison is limited to one value of r, that is, $r = 0.8$. The curves adopted from Fig. 6 show the flutter speed increase ratio, R, for a damped system when the wing mass is taken into account. The other four curves represent the divergence speed according to Eq. (21) divided, for sake of comparison, by the flutter speed of the damped system without wings. The divergence curves for all values of μ nearly coincide over a large range of ε. This is plausible from Eqs. (25) and (26): when the flutter speed is approximated by Selberg's formula, μ cancels in the ratios represented by the curves. For $\mu = 15$, it is seen that divergence becomes governing over flutter for all values of ε considered here. For $\mu = 25$, it is governing for $\varepsilon \leq 1.66$, for $\mu = 40$, it is governing for $\varepsilon \leq 1.32$, and for $\mu = 60$, it is governing for $\varepsilon \leq 1.23$. It is concluded that the strong flutter speed increase achievable by the wings cannot always be fully utilized given that the divergence speed can become smaller than the maximum achievable flutter speed. For economy, the flutter speed should be raised to not more than the divergence speed. This is achieved by reducing the otherwise sensible and possible values of parameters $\tilde{a}_c$, $\tilde{b}_c$, and $\tilde{L}_c$. The variability of these parameters is studied next.

4.5. Girder with full-length wings – variable wing eccentricity or width

Again, wings are added on both sides of the girder along its entire length ($\tilde{L}_c = 1$). Fig. 10 shows the flutter speed increase ratio, R, for a damped system ($g = 0.01$) when the wing mass is taken into account ($\tilde{m}_c = 0.015$), similarly to Fig. 6 but now plotted against the relative wing eccentricity, $\tilde{a}_c$, for selected values of ε and μ and the fixed parameter values $r = 0.8$ and $\tilde{b}_c = 0.1$. All curves increase with $\tilde{a}_c$ and end at a certain final value of $\tilde{a}_c$, even if not visible within the ranges of $\tilde{a}_c$ and R shown here. The curve referring to $\varepsilon = 1.3$, $\mu = 15$, for instance, ends at $\tilde{a}_c = 1.47$, $R = 3.15$. For values of $\tilde{a}_c$ larger than the respective final value, no flutter occurs. The flutter speed increases over-proportionally with $\tilde{a}_c$. With an eccentricity of $\tilde{a}_c = 1$, a noticeable flutter speed increase is achieved only for $\varepsilon = 1.3$, $\mu = 15$. Thus, placing wings directly above the edges of the bridge deck, as suggested by Raggett (1987) and Liu et al. (2006), is mostly not worthwhile. From Figs. 9 and 10, values of $\tilde{a}_c$ can be determined for given parameters ε and μ so that the flutter speed equals the divergence speed. For $\varepsilon = 1.3$, $\mu = 15$, it is seen from Fig. 9 that this condition is met when the flutter speed increase ratio is 1.63. According to Fig. 10, this increase ratio is achieved with $\tilde{a}_c = 1.27$. For $\varepsilon = 1.7$, $\mu = 15$, both speeds coincide at a flutter speed increase ratio of 1.40, leading to a corresponding relative wing eccentricity of $\tilde{a}_c = 1.57$. Based on these considerations, and taking into account previous design and cost studies for the wings and their support structures (Starossek et al., 2018), a wing eccentricity in the range $1.5\ (\text{or}\ 1.3) \leq \tilde{a}_c \leq 2.0$ appears reasonable, where the lower limit 1.3 holds for $\varepsilon \approx 1.3$, $\mu \approx 15$. When choosing $\tilde{a}_c < 1.5$, costs tend to be reduced under-proportionally because of the vertical offset of the wings that is required anyway.

Fig. 11 shows the flutter speed increase ratio, R, for an undamped system when the wing mass is neglected plotted against the relative wing width, $\tilde{b}_c$, for selected values of ε and μ and the fixed parameter values

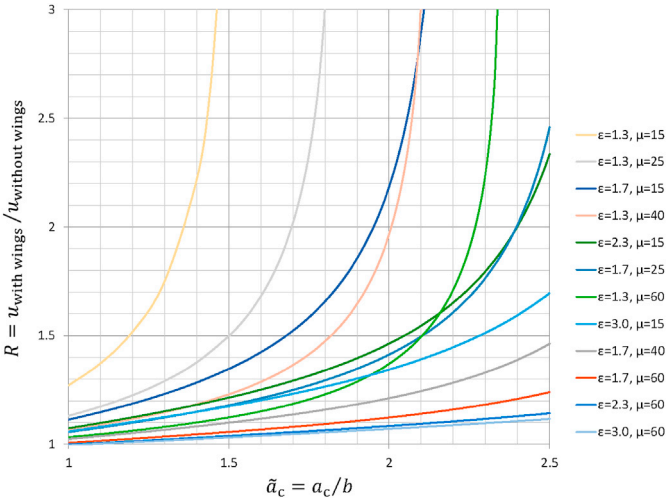

Fig. 10. Flutter speed increase ratio, R, for damped system, wing mass considered, against relative wing eccentricity, $\tilde{a}_c$ ($r = 0.8$, $g = 0.01$, $\tilde{b}_c = 0.1$, $\tilde{L}_c = 1$, $\tilde{m}_c = 0.015$).

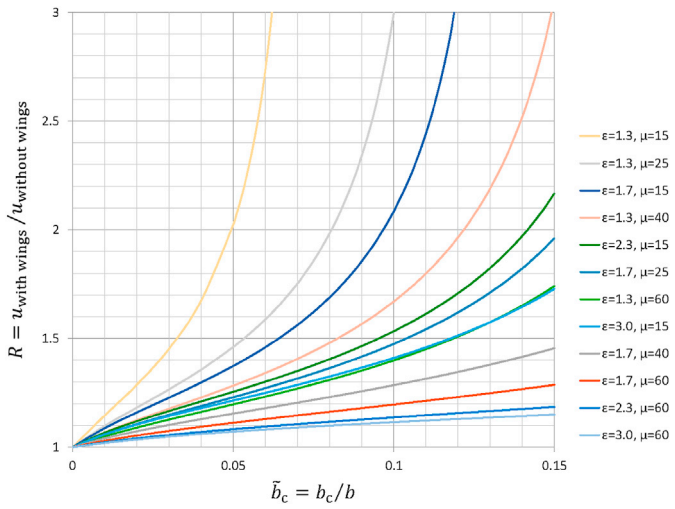

Fig. 11. Flutter speed increase ratio, R, for undamped system, wing mass neglected, against relative wing width, $\tilde{b}_c$ ($r = 0.8$, $\tilde{a}_c = 2.0$, $\tilde{L}_c = 1$).

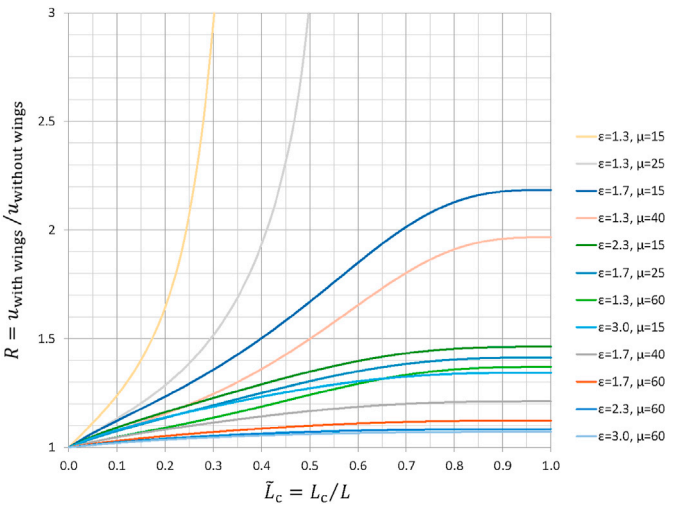

Fig. 12. Flutter speed increase ratio, R, for damped system, wing mass considered, against relative wing length, $\tilde{L}_c$ ($r = 0.8$, $g = 0.01$, $\tilde{a}_c = 2.0$, $\tilde{b}_c = 0.1$, $\tilde{m}_c = 0.015$).

$r = 0.8$ and $\tilde{a}_c = 2.0$. Similar characteristics as in Fig. 10 are present: the flutter speed increases over-proportionally, although not always and to a lesser degree, with $\tilde{b}_c$, and the curves end at a certain value of $\tilde{b}_c$ above which no flutter occurs (not shown). Again, values of $\tilde{b}_c$ can be determined so that the flutter speed equals the divergence speed. For $\varepsilon = 1.3$, $\mu = 15$, with the flutter speed increase ratio of 1.63 taken from Fig. 9 (an approximation because Fig. 9 refers to the damped system), a relative wing width of $\tilde{b}_c = 0.038$ follows from Fig. 11. For $\varepsilon = 1.7$, $\mu = 15$, the respective value becomes $\tilde{b}_c = 0.053$. In view of the large eccentricity of $\tilde{a}_c = 2$, such small values of $\tilde{b}_c$ may not be economical, and it seems better to achieve a reduction of the flutter speed increase ratio in another way than by reducing $\tilde{b}_c$. For cost efficiency, a wing width should be chosen that harmonizes with the wing eccentricity such as, for instance, $\tilde{b}_c = \tilde{a}_c/20$.

4.6. Girder with variable-length wings

The flutter speed increase ratio, R, is now considered as a function of the relative wing length, $\tilde{L}_c$, for selected values of ε and μ and the fixed parameter values $r = 0.8$, $\tilde{a}_c = 2.0$, and $\tilde{b}_c = 0.1$. Identical wings are placed on both sides of the girder and they are centred in relation to midspan. Fig. 12 shows the resulting curves for a damped system when the wing mass is taken into account ($g = 0.01$, $\tilde{m}_c = 0.015$). For small ε and μ, the curves increase over-proportionally with $\tilde{L}_c$ and end at a certain value of $\tilde{L}_c < 1$ above which no flutter occurs (curve "$\varepsilon = 1.3$, $\mu = 15$" ends at $\tilde{L}_c \approx 0.32$, $R \approx 3.43$; curve "$\varepsilon = 1.3$, $\mu = 25$" ends at $\tilde{L}_c \approx 0.52$, $R \approx 3.48$.). For the other values of ε and μ, the curves show a more linear characteristic for up to $\tilde{L}_c \approx 0.5$ and then rise under-proportionally approaching their respective final value asymptotically at $\tilde{L}_c = 1$.

When the flutter speed increase shall be reduced to bring it in line with the divergence speed, it seems more sensible to achieve this by decreasing $\tilde{L}_c$. For $\varepsilon = 1.3$, $\mu = 15$, the associated flutter speed increase ratio of 1.63 is achieved with a relative wing length of approximately $\tilde{L}_c = 0.20$, as can be read off in Fig. 12. For $\varepsilon = 1.7$, $\mu = 15$, the flutter speed increase ratio of 1.40 is achieved with a relative wing length of $\tilde{L}_c = 0.33$. For $\varepsilon = 1.3$, $\mu = 40$, to give another example, the associated flutter speed increase ratio of 1.76 (see Fig. 9) is achieved with a relative wing length of $\tilde{L}_c = 0.67$.

When $\tilde{L}_c$ is 0 or 1, not only the girder but also the wing properties are constant along the length of the girder and the vertical and torsional vibration mode shapes of the model systems considered here correspond to sine half-waves and hence coincide, not only in a vacuum but also under the influence of motion-induced wind forces. Hence the flutter speed could also be accurately determined by a generalized 2-DOF flutter analysis using identical shape functions for vertical and torsional displacements. This, in turn, corresponds to a 2-DOF flutter analysis in which the parameters of Section 2 are used directly as generalized system properties (Starossek and Starossek, 2021). It is of interest how the vibration modes change for $0 < \tilde{L}_c < 1$ (studied next) and to what extent the accuracy of a 2-DOF flutter analysis is affected (examined in Section 5).

Fig. 13 shows the torsional component $\alpha(x)$ of the flutter mode shape (eigenvector) for the parameter combination $\varepsilon = 1.3$, $\mu = 15$, $\tilde{L}_c = 0.20$ just addressed, where $0 \le x \le L$ = position variable. The flutter eigenvector has been normalized so that the (non-dimensional) vertical component $h(x)/b$ at midspan is 1. The imaginary part of the vertical component at other locations is very small (≈ 0.0004) so that the real part and the absolute value of the vertical displacement function virtually coincide. Furthermore, both functions are very close to a sine half-wave (maximum difference ≈ 0.0001). As seen in Fig. 13, the absolute value of the torsional displacement function also closely resembles a sine half-wave (maximum relative difference ≈ 0.01). Nevertheless, the torsional displacement function is now intrinsically complex, that is, it can no longer be normalized to a real function, in contrast to a system with $\tilde{L}_c = 0$ or 1. This can be seen from the curve representing the argument of the torsional displacement function, which is noticeably variable and becomes (absolutely) larger at midspan. At all locations, the torsional displacement lags behind the vertical displacement. However, the aerodynamic damping produced by the wings is concentrated around midspan and leads to a larger phase shift at this location. That the torsional displacement function is intrinsically complex is also evident in its real part, which, in contrast to the imaginary part, differs visibly from a sinusoid. The curve representing the ratio of the absolute values of torsional and vertical displacements also appears slightly variable. It becomes greater at midspan, which is ascribed to the concentration of wing mass around this location.

For larger $\tilde{L}_c$, retaining all other parameters, the peculiarities observed in Fig. 13 become more pronounced. Fig. 14 shows the torsional component $\alpha(x)$ of the flutter mode shape for $\tilde{L}_c = 0.32$. As noted above, this value approximately marks the end of the curve "$\varepsilon = 1.3$, $\mu = 15$" in Fig. 12 above which no flutter occurs. (The final value is actually somewhat higher due to the chosen $\tilde{L}_c$ increment; see below.) The same

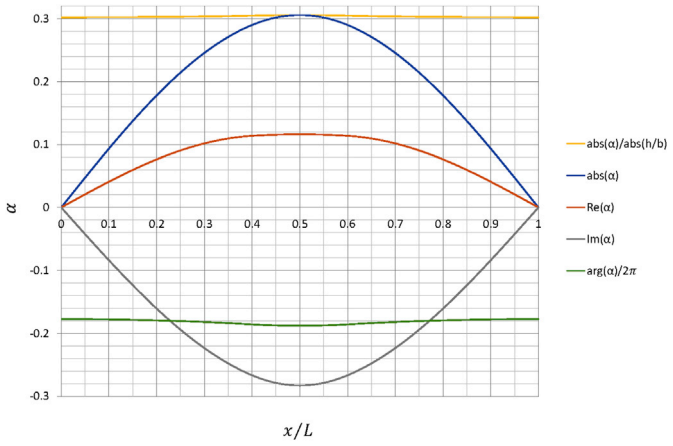

Fig. 13. Torsional component of flutter mode shape for $\varepsilon = 1.3$, $\mu = 15$, $r = 0.8$, $g = 0.01$, $\tilde{a}_c = 2.0$, $\tilde{b}_c = 0.1$, $\tilde{L}_c = 0.20$, $\tilde{m}_c = 0.015$.

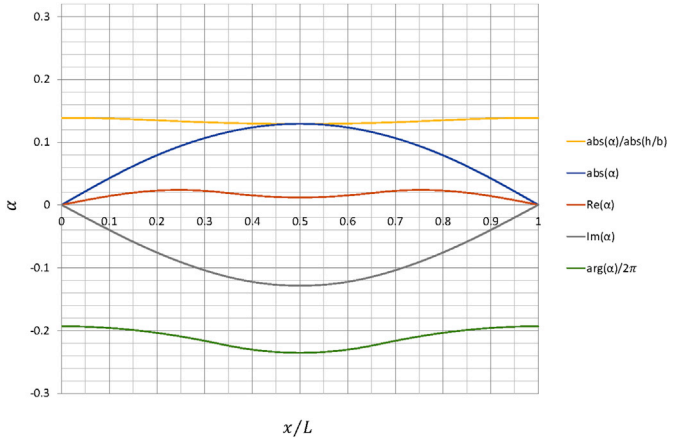

Fig. 14. Torsional component of flutter mode shape for $\varepsilon = 1.3$, $\mu = 15$, $r = 0.8$, $g = 0.01$, $\tilde{a}_c = 2.0$, $\tilde{b}_c = 0.1$, $\tilde{L}_c = 0.32$, $\tilde{m}_c = 0.015$.

normalization is used as for Fig. 13. The imaginary part of the (non-dimensional) vertical component is again very small ($\approx$ 0.0005). The real part and the absolute value of the vertical displacement function are again close to a sine half-wave (maximum difference $\approx$ 0.002). As indicated by the curve showing the torsional displacement argument, the phase shift within the torsional displacement is now rather strong. The real part of the torsional displacement function is clearly indented at midspan, which hints at a greater involvement of the 2nd symmetric torsional vacuum mode (4th mode of vibration in vacuum). The curve representing the ratio of the absolute values of torsional to vertical displacements now becomes smaller, instead of greater, at midspan. This is ascribed to the aerodynamic damping produced by the wings at this location that mainly affects the torsional component (see Section 5) and, due to the higher wind speed, has now become larger and outweighs the effect of the wing mass. The larger aerodynamic damping of the torsional motion component also explains why it has become smaller relative to the vertical component, and its phase shift greater, compared to Fig. 13.

Concerning the curves in Fig. 12 that reach their final value at $\tilde{L}_c = 1$, the torsional components of the respective flutter mode shapes likewise become intrinsically more complex with increasing $\tilde{L}_c$. However, this tendency is reversed at a certain $\tilde{L}_c$ so that the intrinsic complexity of the torsional component finally disappears at $\tilde{L}_c = 1$ (the torsional displacement still lags behind the vertical one). Thus, it is found that for $0 < \tilde{L}_c < 1$ the vertical and torsional components of the flutter mode shape cease to coincide, independently of the girder and wing parameters.

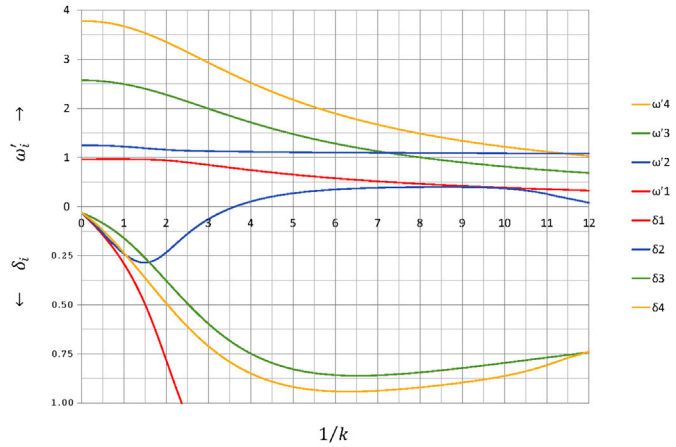

Fig. 15. Complex eigenfrequencies against reduced wind speed, $1/k$, for $\varepsilon = 1.3$, $\mu = 15$, $r = 0.8$, $g = 0.01$, $\tilde{a}_c = 2.0$, $\tilde{b}_c = 0.1$, $\tilde{L}_c = 0.20$, $\tilde{m}_c = 0.015$.

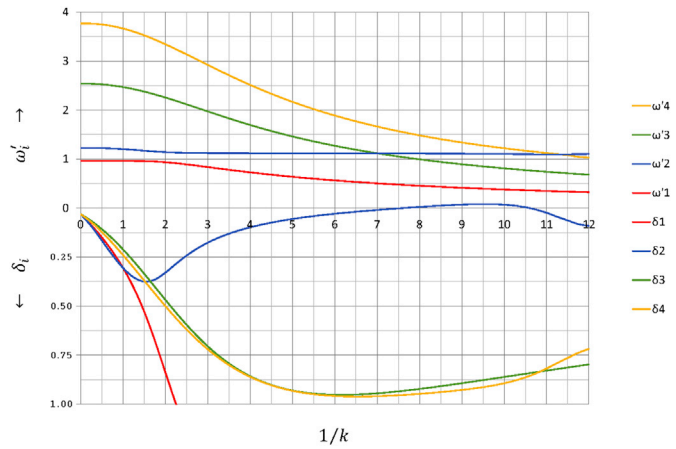

Fig. 16. Complex eigenfrequencies against reduced wind speed, $1/k$, for $\varepsilon = 1.3$, $\mu = 15$, $r = 0.8$, $g = 0.01$, $\tilde{a}_c = 2.0$, $\tilde{b}_c = 0.1$, $\tilde{L}_c = 0.32$, $\tilde{m}_c = 0.015$.

Figs. 15 and 16 show the first four eigenfrequencies, ω_i, plotted against the reduced wind speed, $1/k$, for the two cases just considered in detail, that is, $\tilde{L}_c = 0.20$ and $\tilde{L}_c = 0.32$. The real parts, ω_i' [1/s], appear above the zero line. Below the zero line, the logarithmic decrements, δ_i, are shown, which, according to

$$\delta_i = 2\pi \frac{\omega_i''}{\omega_i'} \tag{27}$$

arise from and represent the respective imaginary parts, ω_i''. For $\tilde{L}_c = 0.20$, the δ_2 branch crosses the zero line at $1/k = 3.6327$ (Fig. 15). This crossing marks the flutter condition. It is associated with $\tilde{\omega} = \omega_2'/\omega_h = 1.1187$, $\zeta = 4.0640$, $R = 1.6439$, and the flutter mode shape shown in Fig. 13. The ω_1' and ω_2' branches approach each other at around $1/k = 2$. This approach normally goes along with the zero crossing of the δ_2 branch so that, normally, the flutter speed would be smaller. However, due to the aerodynamic damping added by the wings, the δ_2 branch is pushed downwards so that the crossing shifts to a higher value of $1/k$.

With $\tilde{L}_c = 0.32$, the aerodynamic damping is further increased. While the ω_i' branches hardly change, the δ_2 branch is further pushed downwards (Fig. 16). Consequently, its zero crossing shifts to the still higher value $1/k = 7.6308$, associated with $\tilde{\omega} = 1.1123$, the much greater non-dimensional flutter speed and flutter speed increase ratio, $\zeta = 8.4874$ and $R = 3.4332$, and the flutter mode shape shown in Fig. 14. A second zero crossing of the δ_2 branch occurs at around $1/k = 10.6$. The

corresponding wind speed is the upper limit of the critical wind speed range. When comparing with Fig. 15, it is seen that the critical $1/k$ and wind speed ranges become smaller when the wing length is increased. When the wings are continuously extended further, the boundaries of the critical range move towards each other, then merge into a point, which finally disappears when the δ_2 branch completely withdraws below the zero line. The merged-point condition marks the wing length above which no flutter occurs. Given the glancing intersection of the δ_2 branch and the zero line, a small increase of wing length above $\tilde{L}_c = 0.32$ suffices to reach the merged-point and no flutter conditions.

It is also seen that the δ_2 branch has a positive curvature in the area of zero crossings. This explains the over-proportional increase of the flutter speed with $\tilde{L}_c$ noted above for small ε and μ (Fig. 12). For larger values of ε and μ, the aerodynamic damping provided by the wings is smaller, relative to the internal system forces, so that even with $\tilde{L}_c = 1$ the aeroelastic system is far from a merged-point condition. The under-proportional and asymptotical approach of the final flutter speed value at $\tilde{L}_c = 1$ noted for such parameter combinations can be explained by the relative ineffectiveness of the wings at the girder ends, where both the vibration amplitudes, and thus the damping forces generated by the wings, and the effectiveness of these forces are small. These relationships are reflected in Eq. (35), the generalization formula given below for taking into account the wing length.

The above explanations based on the positive curvature of the δ_2 branch and the merged-point condition equally apply to the over-proportional increase of the flutter speed with damping in general and $\tilde{a}_c$ and $\tilde{b}_c$ in particular and the ending of the respective curves at a certain value above which no flutter occurs, as noted in Section 4.5.

4.7. Cost efficiency and design

In light bridges with small torsional-to-vertical frequency ratio ($\mu = 15$, $\varepsilon = 1.3$) and streamlined deck, a flutter speed increase ratio of 1.64 is achievable with wing parameters $\tilde{a}_c = 2.0$, $\tilde{b}_c = 0.1$, $\tilde{L}_c = 0.20$, as shown in Section 4.6. This is a higher flutter speed increase at a smaller wing length than found previously in (Starossek et al., 2018) for a heavier bridge and wing parameters $\tilde{a}_c = 2.0$, $\tilde{b}_c = 0.1$, $\tilde{L}_c = 0.50$. For the latter wing parameters, the cost of wings and support structures was estimated on the basis of detailed engineering design studies. The cost relative to the cost of bridge deck and cables was found to be 2.5% for a bridge with a mass ratio of $\mu = 20$ (Starossek et al., 2018). On this basis, the relative cost associated with wing configuration $\tilde{a}_c = 2.0$, $\tilde{b}_c = 0.1$, $\tilde{L}_c = 0.20$ is estimated at $(0.20/0.50)\cdot(20/15)\cdot 2.5\% = 1.3\%$ for a bridge with the above considered parameters ($\mu = 15$, $\varepsilon = 1.3$). The flutter speed increase achieved with this expenditure is 64%. In bridges that are heavier or have a larger torsional-to-vertical frequency ratio, the cost efficiency is smaller but can still be competitive.

The basic design of the wings is defined by the choice of the three parameters $\tilde{a}_c$, $\tilde{b}_c$, and $\tilde{L}_c$, when it is assumed that a symmetric wing configuration with identical parameters on both sides of the bridge deck is chosen. The optimum choice of these parameters depends on the properties of the bridge, that is, on parameters ε, μ, and, to a lesser extent, r, and g, and on the aerodynamic contour of the bridge deck. The influence of the bridge parameters is reflected in the results presented here, which are valid for bridges with streamlined deck. For bluff bridge decks, the intrinsic flutter speed of the bridge is usually smaller and hence the flutter speed increase ratio, R, obtained with the same wing configuration is expected to be higher. The wing design also depends on the required flutter speed, which in turn will usually not be chosen higher than the divergence speed.

A cost-efficient design should take into account the sensitivity of flutter speed and cost to the design parameters. The sensitivity to $\tilde{a}_c$ is over-proportional concerning both flutter speed and cost. The influence of $\tilde{b}_c$ on the flutter speed is over-proportional, although not always and to a lesser degree. Its influence on the cost is expected to be linear or under-proportional. That being said, it seems sensible to choose a wing width that harmonizes with eccentricity. The influence of $\tilde{L}_c$ on the flutter speed is over-proportional for small ε and μ. Otherwise it tends to be linear up to $\tilde{L}_c \approx 0.5$. Furthermore, the gradient of the reduction factor F determined below by the generalization formula Eq. (35) as function of $\tilde{L}_c$ becomes smaller than 1.0 for $\tilde{L}_c > 0.50$, meaning that a further increase in wing length is accompanied by a comparatively smaller increase of wing effectiveness. The influence of $\tilde{L}_c$ on the cost is linear.

Based on these considerations, the following design strategy is suggested. The relative wing length is set to $\tilde{L}_c = 0.50$. The relative wing eccentricity, $\tilde{a}_c$, and the relative wing width, $\tilde{b}_c$, are determined such that the required flutter speed is achieved, keeping these two parameters at a fixed ratio of $\tilde{b}_c/\tilde{a}_c = 0.050$. In these calculations, the structural damping is set to $g = 0.01$ (or $\xi = 0.5\%$) and the wing mass to $\tilde{m}_c = 0.015\cdot\tilde{b}_c/0.1$. If the ensuing $\tilde{a}_c$ is less than 1.5 (or 1.3 for small ε, μ, that is, $\varepsilon \approx 1.3$, $\mu \approx 15$), the process is repeated with smaller $\tilde{L}_c$. If $\tilde{a}_c$ is greater than, say, 2.0, it is repeated with larger $\tilde{L}_c$. The entire analysis is redone for another width-to-eccentricity ratio of, say, $\tilde{b}_c/\tilde{a}_c = 0.075$. Preliminary designs and cost estimates are performed and the final wing parameters are chosen.

The wings thus defined are centred in relation to the peak positions of the respective mode shapes to achieve maximum effectiveness. In a three-span suspension bridge, this is the centre of the main span when flutter is governed by lowest symmetric modes of vibration, and the quarter points of the main span when flutter is governed by lowest antisymmetric modes.

5. Two-degree-of-freedom flutter analysis

The question was raised in Section 4.6 as to what extent the accuracy of a 2-DOF flutter analysis is affected by the wing properties not being constant along the length of the girder when $0 < \tilde{L}_c < 1$ and the dissimilarity of the vertical and torsional vibration mode shapes that arises in such a case. To clarify this question, 2-DOF flutter analyses are performed for a few selected cases. The underlying theory is presented in (Starossek and Starossek, 2021). The definitions of Section 2 are adopted. The non-stationary aerodynamic coefficient functions given in Theodorsen (1934), Starossek (1992) are used for the girder. The motion-induced wind forces on the wings and the wing mass are taken into account by modifying the input to a conventional 2-DOF flutter analysis program. In contrast to the above MDOF flutter analyses, the motion-induced wind forces on the wings are not taken into account by using Theodorsen's aerodynamic coefficient functions but assuming quasi-stationary potential flow past a thin flat plate. The error resulting from this simplification is negligible (Starossek and Starossek, 2021).

Accordingly, the rotational structural damping, $g_\alpha = g$, is increased by an aerodynamic damping contribution, $g_{\alpha,c}$, produced by the wings. The wing mass, m_c, is considered by including it in m and I. The wings not extending over the full length of the girder ($0 < \tilde{L}_c < 1$) is taken into account by multiplying the mass and aerodynamic damping contributions of the wings by a reduction factor, F. When identical wing configurations are present on both sides of the girder, the modified input data are obtained from the following expressions.

$$\overline{\omega}_h = \omega_h\left(1 + 2\tilde{m}_c F\right)^{-\frac{1}{2}} \tag{28}$$

$$\overline{\omega}_\alpha = \omega_\alpha\left(1 + 2\tilde{m}_c\tilde{a}_c^2 F \Big/ r^2\right)^{-\frac{1}{2}} \tag{29}$$

$$\overline{\varepsilon} = \frac{\overline{\omega}_\alpha}{\overline{\omega}_h} = \varepsilon\left[\left(1 + 2\tilde{m}_c F\right) \Big/ \left(1 + 2\tilde{m}_c\tilde{a}_c^2 F \Big/ r^2\right)\right]^{\frac{1}{2}} \tag{30}$$

$$\overline{\mu} = \mu\left(1 + 2\tilde{m}_c F\right) \tag{31}$$

$$\overline{r} = r\,\frac{\varepsilon}{\overline{\varepsilon}} \tag{32}$$

$$\overline{g}_h = g_h = g \tag{33}$$

$$\overline{g}_\alpha = g + g_{\alpha,c}; \quad g_{\alpha,c} = \frac{4\tilde{a}_c^2 \tilde{b}_c F}{\overline{\varepsilon}^2 \overline{\mu}\,\overline{r}^2} \cdot \frac{\left(\omega/\overline{\omega}_h\right)^2}{k} = \frac{4\tilde{a}_c^2 \tilde{b}_c F}{\varepsilon^2 \mu r^2} \cdot \frac{\tilde{\omega}^2}{k} \tag{34}$$

Hence the structural damping of vertical motion input quantity, g_h, remains unchanged. The reduction factor results from generalization of the actual system and reads

$$F = \frac{\int_{x_a}^{x_b} \sin^2(\pi x/L)dx}{\int_0^L \sin^2(\pi x/L)dx} = \tilde{L}_c + \frac{1}{\pi}\sin \pi \tilde{L}_c \tag{35}$$

where x = position variable, x_a = starting position of wing, x_b = end position of wing. A sine half-wave is selected as shape function in the generalisation, which corresponds to the flutter mode shape of the considered simply supported girder if $\tilde{L}_c = 0$ or 1. The final term in Eq. (35) results from centring the wings in relation to midspan. The reduction factor is 1 for $\tilde{L}_c = 1$. Eq. (34) contains the reduced frequency, k, and either the circular flutter frequency, ω, or the non-dimensional flutter frequency, $\tilde{\omega}$, which are unknown at the beginning of the calculation. Hence the 2-DOF analysis procedure described here requires iteration.

A 2-DOF flutter analysis is performed for a parameter combination already studied in Section 4.6:

$$\varepsilon = 1.3; \quad \mu = 15; \quad r = 0.8; \quad g = 0.01 \tag{36}$$

$$\tilde{a}_c = 2.0; \quad \tilde{b}_c = 0.1; \quad \tilde{L}_c = 0.20; \quad \tilde{m}_c = 0.015$$

The reduction factor according to Eq. (35) is $F = 0.38710$ and the modified input data according to Eq. (28) and Eqs. (30)–(34) are

$$\begin{aligned} &\overline{\omega}_h = 0.9942\,\frac{1}{\mathrm{s}}; \ \overline{\varepsilon} = 1.2625; \quad \overline{\mu} = 15.174; \quad \overline{r} = 0.8238 \\ &\overline{g}_h = 0.01; \quad \overline{g}_\alpha = 0.01 + 0.038175 \cdot \frac{\tilde{\omega}^2}{k} \end{aligned} \tag{37}$$

The following results are obtained in the last iteration step.

$$\begin{aligned} &\overline{g}_\alpha = 0.19062 \ \Rightarrow \ k = 0.25896; \quad \tilde{\omega} = 1.1069; \quad \zeta = 4.2744 \\ &\Rightarrow \ \overline{g}_\alpha = 0.19062 \end{aligned} \tag{38}$$

The more accurate results obtained from MDOF flutter analysis were

$$k = 0.27528; \quad \tilde{\omega} = 1.1187; \quad \zeta = 4.0640 \tag{39}$$

Hence the 2-DOF flutter analysis overestimates the flutter speed by 5.2%.

When $\tilde{L}_c$ is increased, retaining all other parameters, the inaccuracy of the 2-DOF analysis likewise increases, always overestimating the flutter speed. For $\tilde{L}_c = 0.28$, the error is 29.0%. For $\tilde{L}_c = 0.32$, the iteration of the 2-DOF flutter analysis procedure does not converge to a finite solution, in contrast to the MDOF flutter analysis that yields a high but finite flutter speed (see Section 4.6). The growing error is attributed to the increasing deviation of the torsional component of the flutter mode shape (Figs. 13 and 14) from the vertical component and from the sine half-wave shape function used in the generalization – explicitly for the wing-produced forces, Eq. (35), and implicitly for the other forces. The increasing deviation, in turn, results from the wing properties not being constant and hence a concentration of wing-produced damping forces over a certain length at midspan, which directly only affect the torsional motion component and grow with wind speed.

6. Conclusions

The flutter speed of a bridge can be raised by wings that are eccentrically attached to the bridge deck. The flutter speed increase depends on the wing configuration and on the properties of the bridge. It is highest for light bridges with small torsional-to-vertical frequency ratio. For certain bridges and wing configurations, the flutter speed can be more than doubled or flutter can be suppressed entirely by the wings. The cost associated with a flutter speed increase of 64% was found to be as small as 1.3% of the cost of bridge deck and cables. The wings do not need to extend over the full length of the bridge and can be placed where they are most effective – a freedom of design not available in the twin deck concept. The results presented here are valid for bridges with streamlined deck. The flutter suppression effectiveness and cost efficiency of the wings are expected to be higher for bridges with bluff deck.

The influence of the wing eccentricity on the flutter speed is found to be over-proportional. The influence of the wing width is partly over-proportional. For both parameters, upper limit values exist above which no flutter occurs. The influence of the wing length on the flutter speed is strongly over-proportional for light bridges with small torsional-to-vertical frequency ratio. In these cases, upper limit values exist above which no flutter occurs so that the maximum possible flutter speed is achieved with wing lengths smaller than the bridge length. In other cases, the maximum flutter speed is approached asymptotically when the wing length approaches the length of the bridge. When the wing mass is taken into account in the analysis, the flutter speed increase due to the wings can be lower or higher, depending on the bridge and wing parameters. For the parameter space considered here, the maximum reduction is 8%. The reasons underlying all these phenomena were discussed.

Based on these findings and on cost considerations, a strategy for the cost-efficient choice of the eccentricity, width, and length of the wings for achieving a required flutter speed is suggested. The required flutter speed will usually not be chosen higher than the critical wind speed for torsional divergence. Because of this, the otherwise achievable maximum flutter speed increase often cannot be utilized to the full.

The numerical results presented here are obtained by multi-degree-of-freedom (MDOF) flutter analysis. Additionally, generalized two-degree-of-freedom (2-DOF) flutter analysis is performed and the results are compared to those of the MDOF analysis. This allows conclusions about the validity of the 2-DOF generalization in case the wing length is less than the bridge length.

CRediT authorship contribution statement

Uwe Starossek: Conceptualization, Methodology, Software. **Rudolf T. Starossek:** Methodology, Software, Numerical computation.

Declaration of competing interest

The authors declare that they have no known competing financial interests or personal relationships that could have appeared to influence the work reported in this paper.

References

Brancaleoni, F., et al., 2010. The Messina Strait Bridge – A Challenge and a Dream. Stretto di Messina S.p.A. CRC Press/Balkema, Rome.
Bruno, D., Leonardi, A., Maceri, F., 1987. On the nonlinear dynamics of cable-stayed bridges. In: Proc., Int. Conf. Cable-Stayed Bridges, Bangkok, vol. 1, 529–544.
Clough, R.W., Penzien, J., 1975. Dynamics of Structures. McGraw-Hill, New York.
Diana, G., Fiammenghi, G., Belloli, M., Rocchi, D., Resta, F., Zasso, A., 2007. Sensitivity analysis on the effects of different aerodynamic devices on the behavior of a bridge deck. In: Proc., 12th International Conference on Wind Engineering, Cairns, Australia, vol. 2, pp. 2191–2198.
Ewert, S., 2003. Brücken – Die Entwicklung der Spannweiten und Systeme. Ernst & Sohn, Berlin.
Farquharson F.B., Smith F.C., Vincent G.S., 1949. Aerodynamic Stability of Suspension

Bridges with Special Reference to the Tacoma Narrows Bridge. Part I-V, University of Washington, Engineering Experiment Station, Bulletin vol. 116, Seattle; 1949–1954.
Försching, H.W., 1974. Grundlagen der Aeroelastik. Springer Verlag, Berlin.
Fuchida, M., Kurino, S., Kitagawa, M., 1998. Design and construction of the Akashi Kaikyo bridge's superstructure. International Association for Bridge and Structural Engineering, Report 79, pp. 63–68.
Larsen, A., 1993. Aerodynamic aspects of the final design of the 1624 m suspension bridge across the Great Belt. J. Wind Eng. Ind. Aerod. 48, 261–285.
Larsen, A., Jacobsen, A.S., 1992. Aerodynamic design of the Great Belt East Bridge. In: Larsen, A. (Ed.), Aerodynamics of Large Bridges. Proc., First International Symposium on Aerodynamics of Large Bridges, Copenhagen. Balkema, Rotterdam.
Liu, Gao, Meng, Fanchao, Wang, Xiuwei, 2006. Mechanism of flutter control of suspension bridge by winglets. In: Proc., 4th International Symposium on Computational Wind Engineering, Yokohama, Japan.
Meyer, S.C., 2019. Buffeting-Induced Fatigue Analysis of a Flutter-Stabilizing Device for Bridges [Master Thesis]. Structural Design Laboratory, Seoul National University; Structural Analysis Institute, Hamburg University of Technology.
Miyata, T., Yokoyama, K., Yasuda, M., Hikami, Y., 1992. Akashi Kaikyo Bridge: wind effects and full model wind tunnel tests. In: Larsen, A. (Ed.), Aerodynamics of Large Bridges. Proc., First International Symposium on Aerodynamics of Large Bridges, Copenhagen. Balkema, Rotterdam.
Ostenfeld, K.H., Larsen, A., 1992. Bridge engineering and aerodynamics. In: Larsen, A. (Ed.), Aerodynamics of Large Bridges. Proc., First International Symposium on Aerodynamics of Large Bridges, Copenhagen. Balkema, Rotterdam.
Raggett, J.D., 1987. Stabilizing winglet pair for slender bridge decks. Bridges and transmission line structures. In: ASCE Structures Congress, Orlando, Florida.
Richardson, J.R., 1981. The Development of the Concept of the Twin Suspension Bridge. Report 125. National Maritime Institute, NMI R, Feltham, UK.
Salcher, P., Pradlwarter, H., Adam, C., 2014. Reliability of high-speed railway bridges with respect to uncertain characteristics. In: Proc., 9th International Conference on Structural Dynamics, EURODYN 2014, Porto.
Selberg, A., 1961. Oscillation and Aerodynamic Stability of Suspension Bridges. Acta Polytechnica Scandinavica, Civil Engineering and Building Construction Series No. 13 (308/1961), Trondheim.
Starossek, U., 1992. Brückendynamik – Winderregte Schwingungen von Seilbrücken. Friedr. Vieweg & Sohn, Braunschweig/Wiesbaden. https://www.tuhh.de/alt/sdb.
Starossek, U., 1993. Prediction of bridge flutter through use of finite elements. Structural Engineering Review 5 (4), 301–307. https://www.tuhh.de/alt/sdb.
Starossek, U., Aslan, H., 2008. Passive control of bridge deck flutter using tuned mass dampers and control surfaces. In: Proc., 7th European Conference on Structural Dynamics, EURODYN 2008, Southampton, UK.
Starossek, U., Ferenczi, T., Priebe, J., 2018. Eccentric-wing flutter stabilizer for bridges – analysis, tests, design, and costs. Eng. Struct. 172, 1073–1080. https://doi.org/10.1016/j.engstruct.2018.06.056.
Starossek, U., Starossek, R.T., 2021. Flutter analysis methods for bridges stabilized with eccentric wings. Preprint, Structural Analysis Institute, Hamburg University of Technology. https://www.tuhh.de/alt/sdb.
Theodorsen, T., 1934. General Theory of Aerodynamic Instability and the Mechanism of Flutter. NACA. Technical Report No. 496.
Yamaguchi, H., Fujiwara, T., Yamaguchi, K., Matsumoto, Y., Tsutsumi, K., 2004. Coupling of cable vibration and its damping effect in long-span cable-stayed bridge: the Tatara Bridge. Civil Eng. Soc. Jpn. Proc. 7, 309–323.
Yanaka, Y., Takazawa, T., Hirahara, N., 1998. Erection of the Tatara bridge's superstructure. International Association for Bridge and Structural Engineering Report 79, pp. 75–80.
Yang, Y., Zhang, L., Ding, Q., Ge, Y., 2018. Flutter performance and improvement for a suspension bridge with central-slotted box girder during erection. J. Wind Eng. Ind. Aerod. 179, 118–124.